International Journal Dental and Medical Sciences Research
Volume 5, Issue 2, Mar - Apr 2023 pp 712-720 www.ijdmsrjournal.com ISSN: 2582-6018

Thermal mapping of osteotomy with osseodensification drills in ex-vivo porcine models and correlations with the Hounsfield unit – analysis in microtomography

Nayra Patrícia da Silva Velasco, BS[1]
Pâmella dos Santos Bastos, BS[1]
Verônica de Mello Soares Frauches, MSc[2]
Victor Talarico Leal Vieira, DSc, MSc, PhD[2]
Fabiano Luiz Heggendorn, DSc, MSc, PhD[2]

[1] *Faculty of Dentistry of the University of Grande Rio (UNIGRANRIO), Rua Prof. José de Souza Herdy, 1160, bloco C, 2º andar - 25 de agosto - Duque de Caxias / Rio de Janeiro, Brazil - CEP: 25071-202.*
[2] *Postgraduate Program in Dentistry, University of Grande Rio (UNIGRANRIO), Rua Prof. José de Souza Herdy, 1160, bloco C, 2º andar - 25 de agosto - Duque de Caxias / Rio de Janeiro, Brazil - CEP: 25071-202.*

Date of Submission: 01-04-2023 Date of Acceptance: 10-04-2023

ABSTRACT
During milling to install dental implants, the bone tissue is heated and can reach nervous structures, such as the inferior alveolar nerve. **Purpose**. The objective of this study was to measure and compare the thermal variations produced during osteotomy with osseodensification drills at different pre-established distances. **Materials and methods**. 4 groups simulated anatomical structures, artificially made in-vitro and ex-vivo in porcine ribs: Atrophic Alveolar Crest (G1), Basilar Medullary (G2), Inferior Alveolar Canal (G3), and Medullary (G4). Thermal variation was correlated with bone density using the Hounsfield unit (HU) and with the different distances between the thermal measurement points and the osteotomy, performed with osseodensification drills at 720 rpm and 20 N/cm^3, without irrigation. **Results**. When performing the paired t-test, the temperatures before and after the osteotomy in groups G1 and G4 are statistically different. The statistical analysis of the mean forces applied during osteotomy did not show a statistically significant difference between the studied groups (p=0.161). The microtomography analysis revealed the average value of the bone mineral density parameter of each sample: 0.358 g.cm^3 (G1), -0.021 g.cm^3 (G2), -0.054 g.cm^3 (G3), and -0.061 g.cm^3 (G4). **Conclusion**. the data demonstrated a direct relationship between bone density and temperature increase during osteotomy. There was a direct relationship between the increased use of force during osteotomy and bone density, requiring greater force in regions with higher bone density (p<0.05).

KEYWORDS: Milling, dental implants, inferior alveolar nerve.

I. INTRODUCTION

The influence of temperature generated during osteotomy on the successful osseointegration of a dental implant is widely discussed[1-3]. The high temperature in the bone can lead to failure to achieve osseointegration by causing hyperemia, necrosis, fibrosis, cell degeneration, and increased osteolytic activity[1]. Eriksson & Albrektsson[4] in 1984 stated that bone repair is affected by the heat generated during preparation for implant placement. Different factors may cause bone tissue heating, such as rotational speed, anatomical characteristics of the cutters, pressure exerted on the cutter, irrigation system used, bone density, and depth and type of perforation[2,5-9]. Bone tissue is sensitive to temperature variations, which can cause cellular damage harmful to osseointegration[1]. The bone type is relevant and should be known because the denser it is, the greater the temperature increases. The cortical bone is denser and presents less water than the medullary bone, demonstrating resistance during milling[1,2]. The bone marrow has faster thermal conduction once it contains more water and lipids, so the heat generated by friction does not dissipate easily to the bone end. The trabecular bone is a spongy and less dense region where the bone trabeculae are located[2].

Studies differ on the factors that interfere with the temperature generated in the bone during the bed preparation for an implant installation. Chacon et al.[7] stated that systems requiring fewer

cutters to drill the bone generates more heat in the bone structure. Sharawy et al.[8] demonstrated the relationship between heating and drilling time during bed preparation, concluding that the tension imposed on the cutter changes the temperature. Another factor cited in the literature is the depth of perforation, demonstrating a direct relationship between perforation depth and local heat generation[9]. Currently, the most defended factor by the dental community is that the drilling speed is what most increases the heat generation in the bone bed; thus, reducing the milling speed would avoid overheating[1].

Therefore, the magnitude of the damage during the installation of osseointegrated implants depends on four factors inherent to the surgical technique: the cutting power of the drills, the bone density, the cutting parameters used, and the continuous irrigation of refrigerant solutions during the execution of the hole[1,2].

The present study aimed to measure and compare the thermal variations produced during osteotomy with osseodensification drills at different pre-established distances, simulating the anatomical structures of the inferior alveolar canal, foraminal exits, and atrophic alveolar crest, generally visualized in resorbed alveoli. The structures were artificially made in-vitro and ex-vivo in porcine ribs. In parallel, we correlated the thermal variation with the bone density determined through the Hounsfield unit (HU) and with the distances between the thermal measurement points and the osteotomy.

II. MATERIAL AND METHODS

This study was submitted to the ethics committee on animal use of the University of Grande Rio (UNIGRANRIO) No. 045/2021. We used four porcine rib bone fragments. The proof bodies (PB) were sectioned to obtain fragments of 5 cm in length, leaving the marrows exposed in the proximal PB.

2.1 PROOF BODIES

Bone PB simulated different distances between osteotomy sites with anatomical structures: inferior alveolar canal and foraminal exits, both artificially created. The atrophic alveolar crest was also considered, as it is routinely visualized in resorbed alveoli.

PB-G1- ATROPHIC ALVEOLAR CREST

This PB received four thermocouple sensors positioned in the cortical vestibular region. Each apical and middle third of the osteotomy had one thermocouple, 1 cm horizontally away from the osteotomy point, in the same axial plane, with the insertion of the milling performed in the center of the distance between the horizontal thermocouple sensors.

The vestibular-lingual positioning of the osteotomy insertion point occurred for the vestibular, simulating an atrophic alveolar crest, with minimal bone volume for insertion of osseointegrated implants, evaluating the possible heat transfer to soft tissues and nerves in atrophic cortical.

PB-G2- BASILAR MEDULLARY

Four perforations in the vestibular cortex to the center of the medullary bone simulated foraminal exits. Each buccal perforation pair was performed in the apical third of the milling point and basilar of the PB, with four thermocouple sensors installed at different transverse distances from the osteotomy perforation point; thereby obtaining data on the medullary bone heating in the apical third of the bone milling point, osteotomy, and in the basilar region of the PB, simulating different positions of the foraminal exit.

PB-G3 – LOWER ALVEOLAR CANAL

Using a 2.0 helical drill, we made a drill at the medullary end of the PB to simulate an inferior alveolar canal. In the canal, two pairs of thermocouple sensors internally touching, each inserted at the mesial and distal ends of the PB, evaluated the internal heating of the inferior alveolar canal during milling.

PB-G4 - Medullary

Four perforations simulated foraminal exits in the vestibular cortex to the center of the medullary bone. The two pairs of vestibular perforations in the apical and middle of the osteotomy accompanied the four thermocouple sensors with different transverse distances from the osteotomy point. Thus, we evaluated the heating of the medullary bone at the different levels of bone osteotomy, middle and apical third of the osteotomy, in addition to simulating different distances from an artificially made foraminal exit.

2.3 THERMAL EVALUATIONS

We fixed the PB in the universal test machine (EMIC DL 200MF) with an adapted implant motor in the load cell of the equipment. The universal testing machine with a load cell of 2 kg/force coupled performed milling. The motor counter-angle was connected to the machine through an apparatus properly developed for the test. The machine performed forward and backward

International Journal Dental and Medical Sciences Research
Volume 5, Issue 2, Mar - Apr 2023 pp 712-720 www.ijdmsrjournal.com ISSN: 2582-6018

movements interspersed with advances of 1mm until it reached a milling depth of 10mm. A Driller engine (BLM350 - Driller) was used. Without irrigation, the motor rotated at a speed of 720 rpm and torque of 20 N.cm^3. During osteotomy, we recorded the forces in four milling points: P1=4mm, P2=6mm, P3=8mm, and P4=10mm.

The temperature was measured throughout the test; a four-channel digital type K thermocouple (HT-9815) inserted in the pre-established areas recorded the maximum thermal peaks. Osseodensifier drills number 2.0 helical, 2.8, and 3.3 Densah Bur (Versah ®) counterclockwise, non-cutting, performed the bone milling sequence to densify the bone and not cut it.

2.4 ANALYSIS IN MICROTOMOGRAPHY

The PB were analyzed through a SkyScan 1172 microtomography (Bruker-µCT, Kontich, Belgium) and correlated the bone density verified in µCT with the thermal variations and distances from the osteotomy points.

The parameters for acquiring images in all stages were: voltage 50 Kvp, Source Current 800 µA, flat-field correction, Image pixel size 28.77 µm, Exposure 4000 ms, rotation step 0.3, 360º rotation, and Al filter 0.5. The images were reconstructed and processed using the NRecon program (SkyScan, Kontich, Belgium).

The reconstructed images were analyzed in the DataViewer program (SkyScan, Kontich, Belgium) for visualization and 2D evaluation of the coronal, transverse, and sagittal axes, using the HU as the imaging unit to correlate the pixel intensity of the specimens with bone density.

The CTan program (SkyScan, Kontich, Belgium) was used to draw the region of interest (ROI), determining the distance between the thermal measurement points and the osteotomy point. Finally, we visually evaluated the 3D images in CtVox software (SkyScan, Kontich, Belgium).

2.5 STATISTICAL ANALYSIS

The strength data recorded throughout the osteotomies in the PB in the Tesc 3.04 program, connected to a universal test machine (EMIC DL 200MF), underwent Shapiro-Wilk normality tests and subsequent analysis of variance (ANOVA), complemented by the Tukey post-hoc test. The temperature analyses before and after installation were subjected to the paired t-test. We adopted a significance level of 5% in all tests. The software GraphPad Prism 5.01 (Graph Pad Software Inc) performed all the tests.

III. RESULTS

In PB-G1, atrophic alveolar crest, the four thermocouples presented a temperature increase. The points closest to the osteotomy area showed greater thermal variations than the points of readings in the corresponding apical region (Tab. 1). The µCT analysis revealed bone densification in the mesial and distal bone margin in the panoramic section throughout the osteotomy (Tab. 2). The analysis of HU indicated a bone density in the osteotomy walls with peaks of 3900 HU, demonstrating a higher density when compared to the peak of 2950 HU of the medullary bone (Fig. 1).

Table 1 – Thermal correlation of distancing of osteotomy points with thermal measurement points.

	Thermal measurement region	**T0**	**Tf**	**ΔT °C**	**Distance between the osteotomy medullary wall and the thermocouple sensor**	**Mean strength (N) during osteotomy**
G1 Model Atrophic Alveolar Crest	Vestibular – Apical 1	+ 26.9°C	+ 27.3 °C	0,4°C	54.2 pixels (2.99 mm)	3.418 ± 3.69
	Vestibular – Middle 1	+ 27.0°C	27.8 °C	+0.8° C	10.1 pixels (0.57 mm)	
	Vestibular – Apical 2	26.7 °C	27.5 °C	+0.8 °C	54.2 pixels (2.99 mm)	
	Vestibular – Apical 2	26.8 ° C	27.9 °C	1,1.c	10.1 pixels (0.57 mm)	
G4 Medullary model	Vestibular – Apical 1	26.3 °C	27.1 °C	+0.8 °C	110.4 pixels (6.32 mm)	3.787 ± 2.69
	Vestibular – Middle 1	25.4 °C	27.1 °C	1.7°C	58.0 pixels (3.32 mm)	
	Vestibular – Apical 2	25.4 °C	25.9 °C	0.5° C	73.0 pixels (4.18 mm)	

International Journal Dental and Medical Sciences Research
Volume 5, Issue 2, Mar - Apr 2023 pp 712-720 www.ijdmsrjournal.com ISSN: 2582-6018

	Vestibular – Middle 2	26.5 °C	27.6 °C	1.1 c	126.9 pixels (7.27 mm)	
G2 Model Basilar Medullary	Vestibular – Apical 1	26.1 °C	26.1 °C	0 °C	30 pixels (1.73 mm)	0.43 ± 0.54
	Vestibular – Basilar 1	26.3 °C	26.3 °C	0 °C	No osteotomy in the plane of the analyzed image	
	Vestibular – Apical 2	26.3 °C	26.3 °C	0 °C	122.3 Pixels (7.07 mm)	
	Vestibular – Basilar 2	26.0°C	26.0°C	0 °C	No osteotomy in the plane of the analyzed image	
G3 Model Inferior Alveolar Canal	Thermocouple sensor 1 Mesial	25.8 °C	27.5°C	1.7°C	33.6 Pixels (1.93 mm)	1.1 ± 0.76
	Thermocouple sensor 2 Distal	27.2 °C	27.4 °C	+0.2 °C		

ΔT – Thermal variation. Reading depth points: P1=4mm, P2=6mm, P3=8mm, and P4=10mm.

Table 2 – Analysis of the Hounsfield unit in the regions of interest.

Region analyzed	**G1**	**G4**	**G2**	**G3**
Osseodensification, Mesial	3900 to -100 HU	3250 to -950 HU	880 to -1190 HU	1940 to -580 HU
Osseodensification, Distal	3400 to - 50 HU	3200 to -1050 HU	1760 to -1170 HU	1940 to -610 HU
Medullary bone density	2950 to -750 HU	2400 to -1300 HU	880 to -1160 HU	1490 to -280 HU
Vestibular cortical bone density	3400 to -250 HU	Not executed	Not executed	Not executed

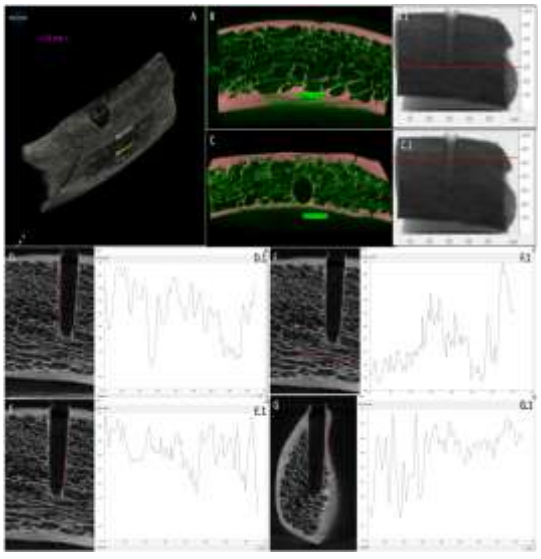

Figure 1 – Analysis in μCT, PB-G1. 3D reconstruction in the Ctvox program demonstrates the insertion point of the thermocouple sensors in the middle third (A, white arrow) and yellow (A, yellow arrow). CTAn program shows the measurement planes of the cortical bone face, from the osteotomy point to the thermal measurement points at the apical level (B and B.1) and the middle third of the perforation (C and C.1). Panoramic slice evaluated by the Data Viewer program (D and E) pointing with the red line the layout of the Hounsfield unit, illustrating a similar pattern between osseodensification and bone density along the mesial and distal margins of the osteotomy, represented in images D1 and E1 respectively. Image F, on the other hand, demonstrates the normal trabecular pattern concerning bone density (F.1), and image G presents the thermal measurement point, showing the relationship between the bone density of the analyzed cortical wall (G.1).

In the basilar medullary PB-G2, the four thermal sensors showed no temperature variations. The distance of the thermal measurement points with the osteotomized bed enabled thermal constancy (Tab. 1). The analysis of the osteotomized bed did not show osseodensification,

International Journal Dental and Medical Sciences Research
Volume 5, Issue 2, Mar - Apr 2023 pp 712-720 www.ijdmsrjournal.com ISSN: 2582-6018

remaining with the same bone pattern surrounding the medullary bone (Fig. 2).

Figure 2 - Analysis in µCT, PB G2. CTAn program, demonstrating the measurement planes of the osteotomized bone wall with the thermal measurement points. Figure A shows the basilar plane of the PB, with the distance between the insertion points of the thermocouples, without the presence of the osteotomized bed between the measurement points (A.1). Image B indicates the image slice in the plane of the apical third of the osteotomized bed, where the measurement was performed on image B.1 and B.2, in the distal and mesial walls, respectively. The Data Viewer program analyzed panoramic Cuts (C, D, and E). The red line indicated in the images corresponds to the reading area of the Hounsfield unit represented in the graphs in the following areas: mesial face (C.1), distal face (D.1), and trabecular pattern between the milling and thermal measurements (E.1).

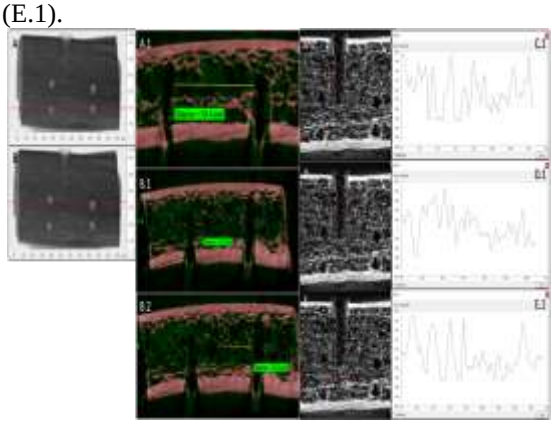

In PB-G3, the two thermal sensors showed thermal variations within the mandibular canal, as shown in table 1 (Fig. 3). However, we did not observe osseodensification in the surrounding walls of the osteotomized bed, presenting the same surrounding bone-medullary pattern (Fig. 3).

Figure 3 - Analysis in µCT, PB-G3. The image presents in the panoramic section the distance between the apical end of the osteotomized bed and the artificial inferior alveolar canal (A). Evaluation of the artificial mandibular canal in the CTAn program, axial section, demonstrating the amplitude and path of the canal (A.1). Panoramic slice analyzed in the DataViewer program (B, C, and D). Images B and C indicate, with a red line, the Hounsfield line represented in graphs B.1 and C.1, respectively. Image D shows the trabecular pattern between the apical end of the osteotomized bed with the artificial inferior alveolar canal, represented in graph D.1.

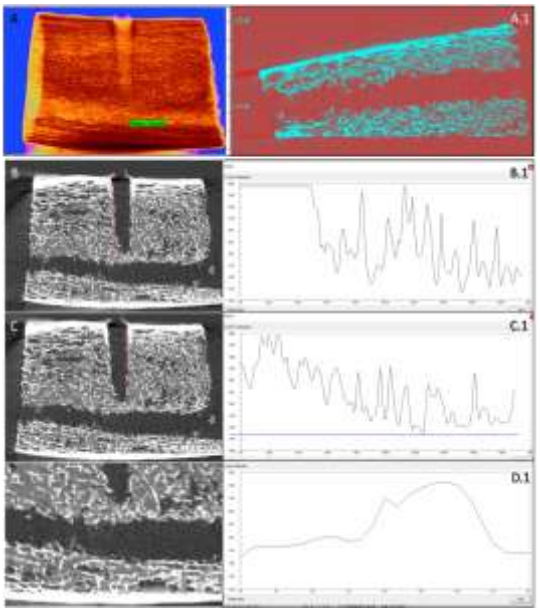

In PB-G4, the four thermal sensors showed an increase in temperature. The readings in the middle third of the osteotomy area showed greater thermal variation compared with the points of readings performed in the apical region. When comparing the two reading regions of the mesial face of the osteotomy, closer to the osteotomized area, with the apical and midpoint of the distal face, the mesial face readings showed greater thermal variation because of the proximity to the milling region (Tab. 1). However, PB-G4 showed no occurrence of osseodensification in the osteotomy region, presenting the same circumjacent medullary bone pattern (Fig.4).

Figure 4 - Analysis in µCT, PB-G4. CTAn program, demonstrating the measurement planes of the osteotomized bone wall with the thermal measurement points. Image A indicates the image crop plane of the performed measurements, in the middle third of the osteotomy, in the distal and mesial walls, respectively (A.1 and A.2). Image B presents the slice plane of the image where the measurements were performed, in the apical third of the milling on distal and mesial walls, respectively (B.1 and B.2). Panoramic cuts (C, D, and E) displayed in the Data Viewer program indicating with the red line the layout of the Hounsfield unit. Images C and D show a similar bone pattern of the margins of the osteotomy point, in the mesial (C) and distal (D) margins with the trabecular circumjacent pattern, through the Hounsfield unit in graphs C.1 and D.1, respectively. Image E exhibits the physiological trabecular bone pattern of the sample, indicating the Hounsfield unit with a red trace (E.1). 3D reconstruction in the Ctvox program demonstrating

International Journal Dental and Medical Sciences Research
Volume 5, Issue 2, Mar - Apr 2023 pp 712-720 www.ijdmsrjournal.com ISSN: 2582-6018

the milling and thermal measurement points (F).

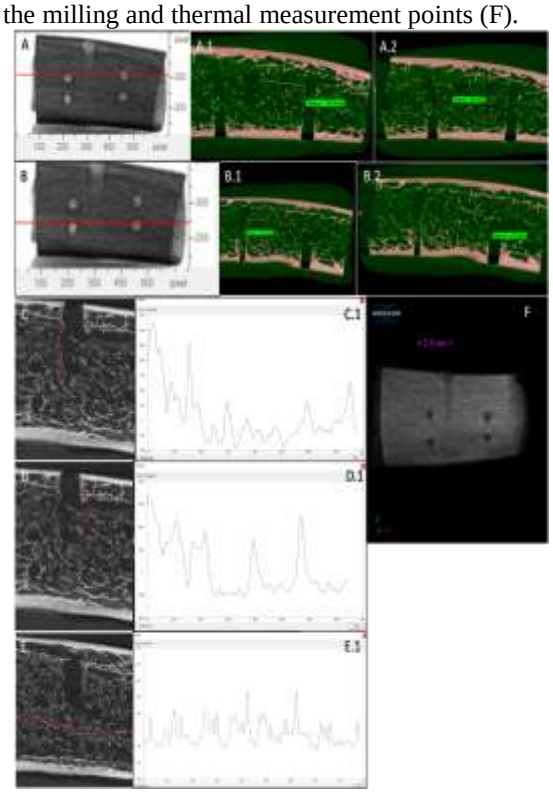

In G1, the mean T_0 was 26.85 ± 0.129, and T_f was 27.62 ± 0.27, whereas the T-test indicated a statistical difference in the initial temperatures and after osteotomy (p=0.012). In G4, the mean T_0 was 25,90 ± 0.58, and T_f was 27.62 ± 0.27, with a significant statistical difference between these temperatures (p=0.028). In G2, both means T_0 and T_f were 26.18 ± 0.15, thus, it did not present a statistical difference between these temperatures (p=0.391). In G3, the mean T_0 was 26.5 ± 0.99 and T_f 27.45 ± 0.07, with no statistical difference between temperatures (p=0.425).

The ANOVA tests for the mean forces applied during the osteotomy of each group did not present any statistically significant differences between the groups (p=0.161).

The mean value of the bone mineral density parameter, defined as the mixture of bone and soft tissue, including all voxels within the volume of interest, was analyzed through the Ctan program. After the reconstruction of each image, we defined the ROI, followed by the binarization of the ROI. After defining the histogram, we obtained the mean value of the bone mineral density parameter of each sample: 0.358 g.cm^3 (G1), -0.021 g.cm^3 (G2), -0.054 g.cm^3 (G3), and -0.061 g.cm^3 (G4).

The ANOVA, with Tukey post-test, of the strength data recorded during the osteotomies of the samples did not indicate the difference between the groups (Graph.1). However, the data suggested a correlation between thermal elevation and increased force exerted during osteotomy in some groups. The PB-G1 showed greater thermal variation in the average buccal cortical area of the milling, +1.1 °C, corresponding approximately to the area of internal osteotomy of the point with greater force reading, P2 (3.60 N) with 6 mm when compared with the most apical points of this sample, P3 and P4. On the other hand, PB-G2 without thermal change after osteotomy presented the lowest strength peaks compared to the same corresponding points in the other groups, excluding P1, which represented the rupture of the cortical bone to start the osteotomy. In addition, these data corroborate with the analysis of the HU that indicated the lower bone density of PB-G2 compared to the other groups.

Graphic 1 – Graphic representation of the strength peaks during the osteotomy of the ex-vivo groups at the different depth points: P1=4mm, P2=6mm, P3=8mm, and P4=10mm.

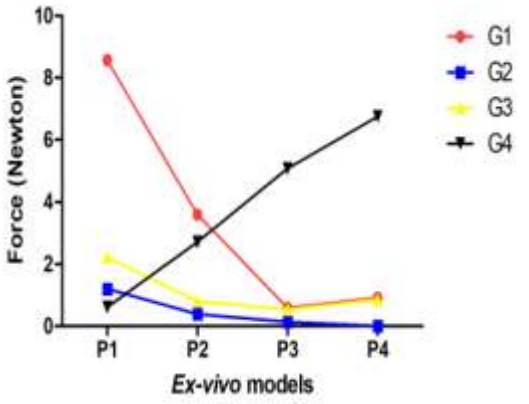

IV. DISCUSSION

In computed tomography, we can obtain results of the tissue attenuation coefficient, making it possible to correlate the characteristics of the tissue types with their density. The lower the density of the tissue, the lower its attenuation coefficient, which can be converted numerically into a scale of values called Hounsfield Units (HU)[11]. The HU represents the amount of radiation absorbed by the body with the function of translating these variations into a grayscale, obtained through a mathematical calculation, based on the attenuation coefficient of previously evaluated substances, such as water with HU equal to zero[12].

Bone density analysis of the PB revealed a higher bone density in PB-G1 (2950 to -750 UH), followed by PB-G4 (2400 to -1300 UH), PB-G3

(1490 to -280 UH), and PB-G2 (880 to -1160 UH) (Table 2). The thermal analysis revealed a statistical difference in PB-G1 and PB-G4, suggesting a relationship between bone density with the thermal change presented in the reading points. When comparing the distances of PB-G1, for example, in the vestibular-apical point 1 with ΔT of +0.4°C and distance of 2.99 mm, with higher values of HU, with PB-G2 with a lower distance of 1.73mm without thermal variation, with the lowest values of HU, corroborates the correlation between the influence of bone density on heating during milling.

The PB-G1, the model with higher medullary bone density, allowed the verification that the intervals of smaller thermal variations are restricted to the largest milling distances (+0.4 °C to +0.8 °C ΔT, distance of 2.99 mm), while a smaller distance represented an increase in the interval of thermal variation (+0.8 °C to +1.1 °C ΔT, distance of 0.5 7 mm). The distance of 1.93 mm from the mandibular canal with the apical point of the osteotomy bed, PB-G3, allowed a thermal reading interval between +0.2 °C and +1.7 °C ΔT. The low bone density of PB-G2 allowed thermal constancy at thermal reading points even at distances lower than the distances reported above (0 °C ΔT, 1.73 mm). In the same group, we adopted higher distances, following the same pattern of absence of thermal variation.

Regarding the osseodensification proposed by the Osseodensifier Kit, the analyses suggested a relationship between bone density with bone compaction. Only in the group with higher cortical bone density an osseodense line could be visually observed in the 3D reconstruction of the images. The design of the osseodensifier drills allows bone particles removed during osteotomy to be compacted against the walls of the alveolus, simulating the compaction of an autogenous graft leading to an increase in bone density, thus resulting in greater primary stability of the implant since this stability is directly related to bone quality and quantity[13,14]. This procedure does not corroborate some aspects of a conventional preparation of an implant bed because it allows the preservation of bone at the osteotomy site.

Comparing the bone density of the milling perforation margins allows the verification, through the Hounsfield line, of a change in bone density in the 4 PB, showing an increase in HU levels compared to medullary HU levels.

The higher medullary bone density indicated higher levels in the HU of osseodensification, demonstrating continuity throughout the milling point, while lower medullary bone densities (G2, G3, and G4) present this discontinuous osseodensification line, with greater evidence at the entrances of the milling point, in the cortical bone.

The Hounsfield value as a quantitative measure to assess bone density can be a great ally for the professional in diagnosing the bone quality before the surgical procedure, facilitating the planning and success of the treatment[11,15,16]. The correlation of HU with bone density allowed us to determine the bone pattern: D1, a dense cortical bone with a HU greater than 1250 HU; D2, a thin cortical bone with a trabecular core, with a HU between 850 and 1250 HU; D3, with a thinner cortical bone and a thin trabecular core, with a HU between 350 and 850 HU; and D4, a bone with almost no inferior cortical bone, with a HU less than 150 HU[1].

Trabecular bones with values lower than 100 HU are classified as of poor, inferior quality, whereas it is difficult to achieve the primary stability of osseointegrated implants[11,17]. Other studies have correlated bone quality with the survival rate of osseointegrated implants through the use of the Hounsfield scale, indicating greater survival in sites with denser bone qualities[18,19].

Bachus et al.[2] evaluated the behavior of the cortical tissue temperature in the peripheral region of the osteotomized bed but considered only the applied force, which in short means changing the progress speed of the process. They concluded that the increased pressure applied during the drilling process greatly decreased the temperature, reducing the drilling time and the time for heat dissipation between the drill and the drilling site.

Misir[10] (2009) compared the generation of drilling heat with the aid of surgical drill guides and classic drilling in cortical bone of the bovine femur. The results revealed relevant temperature differences using thermocouples at a constant load of 2 kg and 1,500 rpm at depths 3, 6, and 9 mm. The average temperatures at the depth points using surgical drill guides were 34.2 °C, 39.7 °C, and 39.8 °C, respectively. Without using guides, temperatures were significantly lower: 28.8 °C, 30.7 °C, and 31.1 °C, respectively. Based on these findings, from the point of view of heat generation, an implant site with surgical guides generates more heat in bone tissue than without guides, regardless of the irrigation system used.

The uncontrolled frictional heat generated during surgical preparation of the bone bed of an implant produces a devitalized bone zone around the perforation. The extent of this necrotic zone varies according to the temperature reached and the duration of the thermal injury. Cordioli &

Majzoub[6], with a cortical bone of the bovine femur, compared the relationship between heat generation and the different types of drills in perforations of 4 mm and 8 mm deep, concluding that the shape of the three-flute drills combines cutting efficiency with greater capacity to dissipate heat in bone tissue than the helical drills, in the depths analyzed.

In 2004, Ercoli et al.[20] studied heat generation and different types of drills, using bovine ribs for 15 mm and 5 mm perforations. The findings suggested no significant correlation between the increase in temperatures and the different types of drills. However, the authors reported clinically harmful temperatures to bone tissue in five osteotomies with a depth of 15mm. Increased milling depth is suggested to be an additional factor in this equation. In the results presented here, a milling depth of 10 mm may have contributed to lower heating between the groups.

Chacon et al.[7] investigated heat production in three different drilling systems, performing several repetitions: triple twist drills with a relief angle, triple twist drills without a relief angle, and double twist drills with a relief angle. Using the technology of thermocouples in the cortical bone of a bovine femur, he performed the perforation with a constant load of 2.4 kg at 2,500 rpm and external irrigation at 40 ml/min with saline solution. The results demonstrated that the unrelieved triple drills reached a temperature above 47 °C, so considered the system of drills generating higher temperatures. The geometry of the drills played an important role in heat generation. The drills that caused the greatest temperature increase did not have a relief angle and had the smallest clearance angles among the drills used in the test. In addition, we also demonstrated that the greater the number of drill reuses, the greater the heat generated in the bone tissue[7].

In 2002, Sharawy et al.[8] conducted a study to measure the heat generated at three different drilling speeds: 1,225, 1,667, and 2,500 rpm, with four implant systems, whereas two systems had external irrigation and two systems had internal irrigation. The perforations were performed on samples of wet porcine jaws, and according to the results obtained, among all the systems, the speed of 2,500 rpm reduced the generation of heat in the bone tissue, reducing the time of preparation of the osteotomy, returning to the original temperature more quickly, especially in the bone regions of higher density. Therefore, in denser bones, the higher speed reduces the drilling time, generating less heat during implant insertion and reducing the devitalized bone area around an implant, increasing the success rates of osseointegration.

V. CONCLUSION

We correlated bone density with temperature increase during osteotomy using osseodensifier drills. We also detected a relationship between increased use of strength during osteotomy and bone density, requiring greater strength in regions with higher density. In addition, the shortest distances between the milled bed and the thermal measurement point presented more effective thermal transport, overheating the reading areas. Therefore, the overheating of the measured regions simulating anatomical structures, inferior alveolar canal, foraminal exits, and atrophic alveolar crest, artificially made in vitro and ex vivo in porcine ribs, depends on multiple factors, such as bone density, suggesting that it is the factor that most influences the overheating.

ACKNOWLEDGEMENTS

National Council for Scientific and Technological Development (CNPQ) and the Research Support Foundation of the State of Rio de Janeiro (FAPERJ).

CONFLICT OF INTEREST

The authors have no conflicts of interest to declare.

REFERENCES

[1]. Misch CE. Implantes dentais contemporâneos, ed 3. Rio de janeiro: Elsevier, 2008.

[2]. Bachus KN, Rondina MT, Hutchinson DT. The effects of drilling force on cortical temperatures and their duration: an in vitro study. Med Eng Phys 2000; 22(10): 685-91.

[3]. Watanabe F, Tawada Y, Komatsu S, Hata Y. Heat distribution in bone during the preparation of implant sites: heat analysis by real-time thermography. Int J Oral Maxillofac Implants 1992; 7(2):212-9.

[4]. Eriksson RA, Albrektsson T. The effect of heat on bone regeneration: an experimental study in the rabbit using the bone growth chamber. J Oral Maxillofac Surg 1984: 42(11):705-11.

[5]. Dodo CG, Sotto-Maior BS, Faot F, Del Bel Cury AA, Senna PM. Lesion in the inferior alveolar nerve by dental implants: prevention, diagnosis and treatment. Dental Press Implantol 2015; 9 (4):57-66.

[6]. Cordioli G, Majzoub Z. Heat generation during implant site preparation: an in vitro study. Int J Oral Maxillofac Implants 1997; 12(2):186-93.

[7]. Chacon GE, Bower DL, Larsen PE, McGlumphy EA, Beck FM. Heat

production by 3 implant drill systems after repeated drilling and sterilization. J Oral Maxillofac Surg 2006; 64(2):265-9.

[8]. Sharawy M, Misch CE, Weller N, Tehemar S. Heat generation during implant drilling: the significance of motor speed. J Oral Maxillofac Surg 2002; 60(10):1160-1168.

[9]. Haider R, Watzek G, Plenk H. Effects of drill cooling and bone structure on IMZ implant fixation. Int J Oral Maxillofac Implants 1993; 8(1):83-91.

[10]. Misir AF, Sumer M, Yenisey M, Ergioglu E. Effect of surgical drill guide on heat generated from implant drilling. J Oral Maxillofac Surg 2009; 67(12):2662-8.

[11]. Shapurian T, Damoulis PD, Reiser GM, Griffin TJ, Rand WM. Quantitative evaluation of bone density using the Hounsfield index. Int J Oral Maxillofac Implants 2006; 21(2):290-7.

[12]. Orhan K. Micro-computed Tomography (micro-CT) in Medicine and Engineering. Switzerland: Springer, 2020.

[13]. Todisco M, Trisi P. Bone mineral density and bone histomorphometry are statistically related. International Journal of Oral and Maxillofacial Implants 2005; 20(6):898–904.

[14]. Trisi P, Perfetti G, Baldoni E, Berardi D, Colagiovanni M, Scogna G. Implant micromotion is related to peak insertion torque and bone density. Clin Oral Implants Res 2009; 20(5):467–471.

[15]. Oliveira RCG, Leles CR, Normanha LM, Lindh C, Ribeiro-Rotta RF. Assessments of trabecular bone density at implant sites on CT images. Oral Surg Oral Med Oral Pathol Oral Radiol Endod 2008; 105(2):231-8.

[16]. Turkyilmaz I, Ozan O, Yilmaz B, Ersoy AE. Determination of bone quality of 372 implant recipient sites using Hounsfield unit from computerized tomography: a clinical study. Clin Implant Dent Relat Res 2008; 10(4):238-44.

[17]. Duckmanton NA, Austin BW, Lechner SK, Klineberg IJ. Imaging for Predictable Maxillary Implants. Int J Prosthodont 1994; 7(1):77-80.

[18]. Fuh LJ, Huang HL, Chen CS, Fu KL, Shen YW, Tu MG, Shen WC, Hsu JT. Variations in bone density at dental implant sites in different regions of the jaw bone. J of Oral Rehabil 2010; 37(5):346–351.

[19]. Hao Y, Zhao W, Wang Y, Yu J, Zou D. Assessments of jaw bone density at implant sites using 3D cone-beam computed tomography. Eur Rev Med Pharmacol Sci 2014; 18(9):1398-403.

[20]. Ercoli C, Funkenbusch PD, Lee HJ, Moss ME, Graser GN. The influence of drill wear on cutting efficiency and heat production during osteotomy preparation for dental implants: a study of drill durability. Int J Oral Maxillofac Implants 2004; 19(3):335-49.